Fracture Toughness of Cemented Carbides Obtained by Electrical Resistance Sintering

Raquel Astacio[a], José María Gallardo[a], Jesús Cintas[a], Juan Manuel Montes[a], Francisco G. Cuevas[b], Leo Prakash[c] and Yadir Torres[a*]

[a]Escuela Técnica Superior de Ingeniería, Universidad de Sevilla, Camino de los Descubrimientos, s/n, 41092 Sevilla, Spain

[b]Escuela Técnica Superior de Ingeniería, Universidad de Huelva, Campus El Carmen, Avda. Tres de Marzo s/n, 21071 Huelva, Spain

[c]Kyocera Unimerco Tooling A/S, Drejervej 2, DK-7451 Sunds, Denmark

*Corresponding author (ytorres@us.es)

Keywords: Electrical Resistance Sintering, Cemented Carbides, Hardmetal, Fracture Toughness

Abstract:

The unique combination of hardness, toughness and wear resistance exhibited by WC-Co cemented carbides (hardmetals) has made them a preeminent material choice for extremely demanding applications, such as metal cutting/forming tools or mining bits, in which improved and consistent performance together with high reliability are required. The high fracture toughness values exhibited by hardmetals are mainly due to ductile ligament bridging and crack deflection (intrinsic to carbides). In this work two WC-Co grades obtained by using the electric resistance sintering technique are studied. The relationships between the process parameters (cobalt volume fraction, sintering current and time, die materials, etc.), the microstructural characteristics (porosity, cobalt volume fraction, carbide grain size, binder thickness and carbide contiguity) and mechanical properties (*Vickers* hardness and fracture toughness) are established and discussed. Also the presence of microstructural anisotropy and residual stresses is studied. The sintering process at 7 kA, 600 ms and 100 MPa, in an alumina die, followed by a treatment of residual stress relief (800 ºC, 2 hours in high vacuum), allows to obtain WC-Co pellets with the best balance between an homogeneous microstructure and mechanical behaviour.

INTRODUCTION

Cemented carbides (WC-Co) are materials used in wide range of applications in many relevant industries, i.e. as cutting tools (turning, milling, drilling) for machining of metal components in the automotive and/or aerospace industry, as components of drill bits or road headers in the rock tools and mining area or as wear parts in wire drawing dies or punch tools, all these applications with stringent requirements [1-3]. Regarding cemented carbides processing, the need to implement more efficient routes than conventional liquid sintering is one of the objectives pursued by the industrial sector. Field-assisted sintering techniques (FAST) have gained particular interest in the last decades [4-6] because of being very quick processes; particularly, the electric resistance sintering (ERS) process [7-9] consists in an electrical current passing through a powder mass to be sintered at the time that pressure is

applied. The Joule effect acts heating and sintering the powders. However, despite its potential advantages, it remains an objective to control the variables associated with the sintering process, as well as to evaluate and rationalize the influence of these variables on the physical and mechanical properties of the manufactured samples.

The influence of the microstructural parameters on the behaviour in service has been widely studied by the scientific-technical community, particularly the mechanical and tribological performance [1, 10-16]. The content and physical dimensions of each constituent phase are the most common features for defining the microstructure [1,10,17]. Within this context, the principal parameters used to characterize the microstructure of hardmetals are the average grain size of WC particles (d_{WC}) and the binder volume content. However, both parameters are frequently varied simultaneously, and correlation between property and microstructure requires of additional two-phase normalizing parameters. Among them, the binder mean free path (λ_{Co}) is the most used one as it refers to the mean size of the metallic phase. In general, an increase of the binder mean free path implies a rise of the fracture toughness of the material at the expense of a decrease in hardness [17,18]. Main reason behind it is the fact that thicker and less constrained (i.e. effectively more ductile) ligaments exist for hardmetal grades with higher binder contents and coarser microstructures [14,15,17,19]. Also, the binder intercept size is an outstanding microstrutural parameter because of its influence on the shear stresses of the material (for example, in cutting tool grades of hardmetal) [20].

Fracture toughness is the most important mechanical property of the WC-Co, considering the intrinsic fragility of these materials. There are different procedures to evaluate fracture toughness of cemented carbides [21-25]. The conventional indentation microfracture [24] is widely used in the literature because of its simplicity, cost and versatility. However, the measured values depend on the equation used, surface preparation, presence of residual stresses and the studied hardmetal grade [24,26,27]. In this context, the main objective of this work is to establish the relationship between the microstructure, the manufacturing process by ERS and the fracture toughness of WC-Co.

MATERIALS AND EXPERIMENTAL PROCEDURE

The starting spherical and rough WC-Co particles are suplied by Kyocera Unimerco Tooling (Denmark) after the adequate powders mixture to achieve the desired composition (see Fig. 1). Two different grades with 6 and 10 wt% Co (binder phase) have been studied in this work.

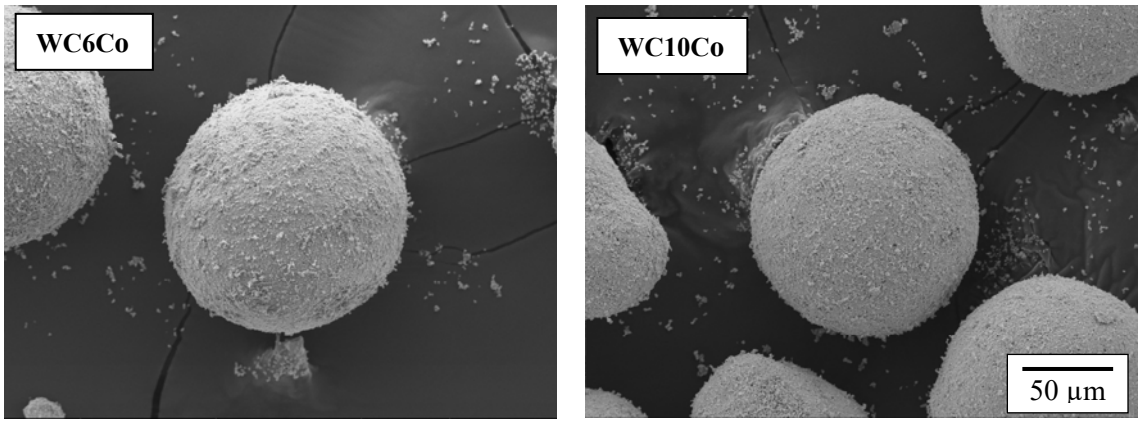

Fig. 1. SEM images of the powders used for the sintering of hardmetals.

Table 1 shows the characteristics of the initial powders (carbon and oxygen content, size, density and flowability of the powders, as well as the relative green density and electrical resistivity for the compaction pressure of 100 MPa applied during electrical sintering). On the other hand, Table 2 summarizes the variables of the electrical resistance sintering process studied in this work.

Table 1. Chemical composition and properties of the starting powders supplied by Kyocera Unimerco (Denmark).

Grade		**WC-6Co**	**WC-10Co**
C (wt%)		5.78	5.52
O (wt%)		0.13	0.12
Spherical WC-Co particles (μm)	**$d_{10\%}$**	86	78
	$d_{50\%}$	141	128
	$d_{90\%}$	225	204
	$D_{[4,3]}$	148	136
Density (g/cm^3)	**Apparent**	15.0	14.5
	Tap	4.4	4.0
Flowability (s/50 g)		19.2	19.7
Compressibility (%)	**100 MPa**	61	63
Electrical resistivity (Ω·m) x 10^{-6}		6.9	6.4

Table 2. Experimental parameters associated to the electrical resistance sintering of the studied WC-Co.

Materials	**Cylindrical die**	Alumina and sialon of high purity and density	
		Internal diameter	12 mm
	Punches	High purity copper	
	Wafers (in powder contact)	Cu-W alloy	
ERS parameters	**Compaction pressure**	100 MPa applied at 100 mm/s	
	Continuous electrical current wave	**Pulse**	Square
		Frequency (MHz)	10
		Intensity (kA)	5 - 10
		Time (ms)	300 - 1000

The WC-Co powder is poured into the cylindrical die. The powder mass used is 6.5 g. The inside walls of the die are previously lubricated with graphite. A single-acting uniaxial pressure is applied to the upper copper punch with the help of an electric actuator. The pressure is maintained during the time that the electric current passes through the powder. Finally, pressure is released 1000 ms after current ceases to allow for compact cooling (Details of ERS process are described elsewhere by the authors [9,28]).

Visual inspection was used for verifying the structural integrity of the samples. Density measurements were carried out by Archimedes' method with distilled water impregnation due to its experimental simplicity and reasonable reliability. The ISO 3369:2006 Standard [29]

gives the details of this protocol. Total porosity was computed from density measurements. The hardness tests were carried out using a *Vickers* indenter Shimadzu (model HMV-G) at 30kgf, according to ISO 3878:1983 [24,30]. Radial cracks were induced from the corners of the Vickers indentation and the arrested crack length was related to the fracture toughness of the WC-Co via relationships of the type $K_{Ic} = \alpha P/ (a \cdot l^{1/2})$, were P is the applied indenter load, a the indentation half diagonal, l the surface *Palmqvist* crack length and α is an empirical, semi-empirical or theoretical constant [31]. The crack length is extremely sensitive to surface preparation [32]. The sectioned WC-Co samples were mounted in resin then ground and diamond polished up to mirror-like surface finish following a 6, 3 and 1 µm sequence, with a final colloidal silica stage [33]. The cracks and porosity observation was performed using a Nikon Epiphot optical microscope coupled with a Jenoptik Progres C3 camera. At least ten measurements were performed per ERS parameters combination and grade material studied. Furthermore, the WC-Co microstructure (cobalt fraction f_{Co}, binder mean free paths λ_{Co}, carbide contiguity C_{WC}, the size and distribution of carbides d_{WC}) was studied in detail by linear intercept method using scanning electron microscopy (SEM, FEI Teneo) and image analysis (Image-Pro Plus 6.2 analysis software). In this work, the used equation for contiguity estimation is based on extensive data collection from literature [33].

RESULTS AND DISCUSSION

Fig. 2 shows photographs and optical micrographs of the axial surface (points 2 and 3 shown in the scheme) of pellets sintered using well apart sintering conditions and alumina die. Also shown are micrographs obtained at different locations of an axial section (points 2 and 3 marked on the macro). The porosity and structural integrity of the sintered pellets vary depending on the hardmetal grade, the electric current and the sintering time. In addition, the porosity distribution is heterogeneous, being higher in the bases and the lateral surface of the pellets, where the punches and die walls act as heat sinks, decreasing the local temperature. As a consequence, the sintered preforms have a relatively porous outer layer that must be removed (ground or machined), the thickness and pore fraction of the surface depends on the energy provided during the process and the WC-Co grade.

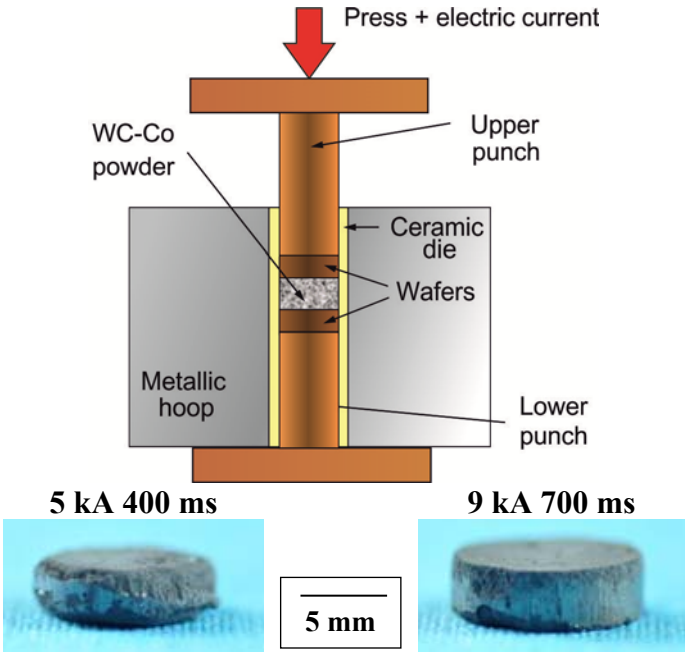

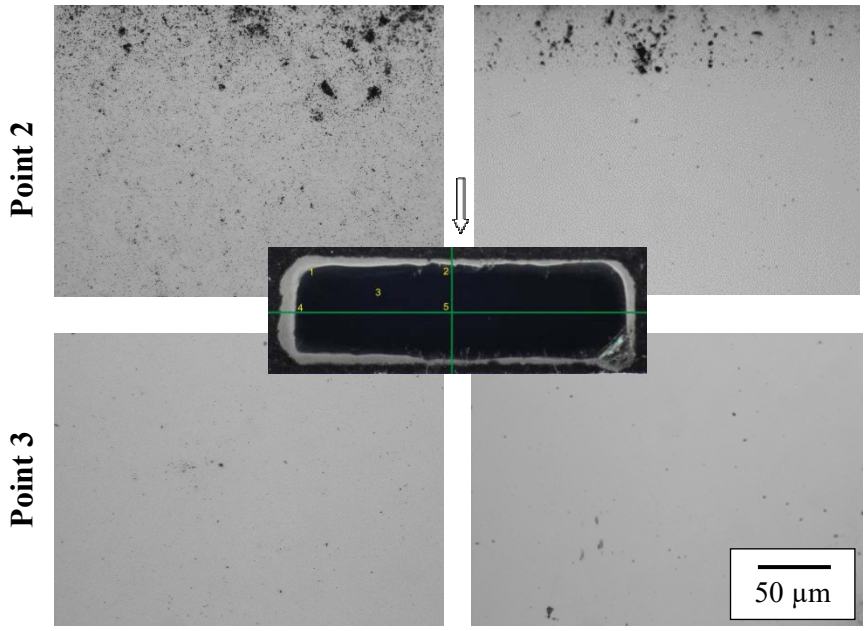

Fig. 2. Structural integrity (photographs) and porosity distribution (optical images – axial surfaces) of the pellets obtained in well apart sintering conditions with the alumina die.

Fig. 3 shows SEM images of pellets obtained using similar processing conditions as described in the previous figure. Typical microstructure of these materials can be observed, with two interpenetrating constitutive phases: equiaxially-shaped, hard and brittle carbides and a soft and ductile metallic binder. Furthermore, Table 3 shows the different microstructural parameters of WC-Co evaluated. The carbide phase contiguity is a key two-phase microstructural parameter to describe the mechanical properties of cemented carbides. In accordance with literature (e.g. Refs. [34,35], contiguity decreases when increasing binder content due to a higher probability of the binder phase to surround ceramic particles. The studied WC-Co grades show nanosized carbide grains and cobalt binder thickness (range of parameters, see table 2). Mean carbides sizes of 300 ± 30 nm and 290 ± 45 nm were measured for WC-6Co and WC-10Co, respectively; while the binder mean free paths were 90 ± 8 nm and 120 ± 16 nm, respectively. In this context, the bulk densities of the sintered pellets (skin and core) vary between 9.0 and 13.5 g/cm^3 for the WC-6Co, and between 9.1 and 12.8 g/cm^3 for the WC-10Co. Particularly, the Figure 3 shows the presence of higher porosity when using lower sintering energy (WC-6Co sintered at 5 kA for 300 ms) and a high density of 12.3 g/cm^3 for higher energy condition (WC-10Co sintered at 9 kA for 400 ms).

Table 3. Experimental parameters of the microstructure of WC-Co studied.

	Grade		**WC-6Co**	**WC-10Co**
	f_{Co}	**wt%**	6	10
		vol%	10.2	16.5
WC-Co sintered	**Cobalt binder thickness (nm)**	λ_{Co}	90 ± 8	120 ± 16
	Carbide contiguity ([24])	C_{WC}	0.64 ± 0.01	0.50 ± 0.02
	Carbide grain size (nm)	d_{WC}	300 ± 30	290 ± 45

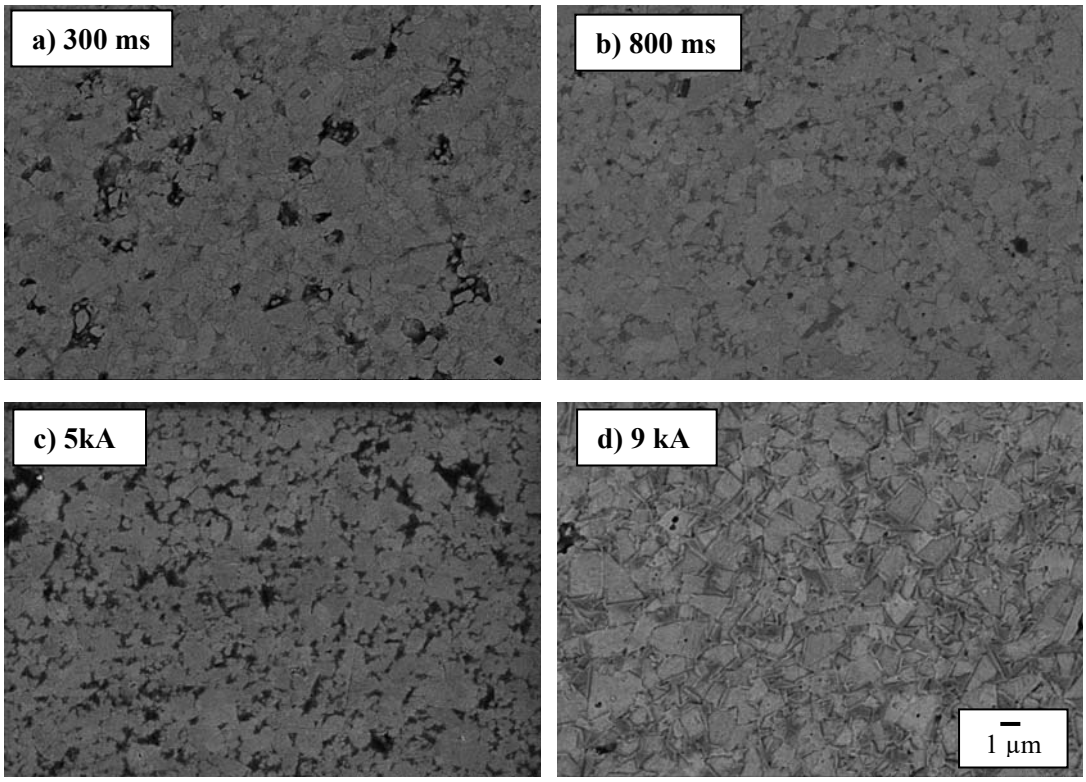

Fig. 3. SEM images of the microstructure of the WC-Co blank core studied (point 3 in the scheme in Figure 2). Influence of sintering time in WC-6Co and 5 kA [a) and b)] and sintering current for WC-10Co and 400 ms [c) and d)].

On the other hand, Fig. 4 shows the *Vickers* hardness and fracture toughness values obtained with the alumina die for the two hardmetal studied (sample core, point 5) depending on current and time processing conditions. In general, the results of this work corroborate the well-known inverse relationship between hardness and fracture toughness. In this context, some other conclusions could also be indicated:

1) As expected, there is a direct relationship between the binder mean free path and the fracture toughness, and an inverse relationship with hardness.

2) Intensive efforts have been carried out by the scientific community to increase hardness and fracture toughness at the same time. The results obtained suggest that a moderate decrease in the applied energy (current and / or time) during the electric sintering process allows the attainment of this balance of mechanical properties. Up to this point, the analysis of the data indicates that the best results were obtained for 6 kA and 500 ms, with values of 1951 HV30 and 11.04 MPa $m^{1/2}$, and 1743 HV30 and 12.14 MPa $m^{1/2}$, for 6 and 10% Co respectively.

3) It is a fact that sintering parameters (current and time) influence the mechanical properties (fracture toughness and hardness). In general, for similar ERS conditions, the range of values of K_{Ic} increase with the cobalt content (path with the least difficulty to pass an electric current), the sintering time being the most significant process parameter. In this above context, note the greater dispersion (less grouped) of the values for the WC-10Co grade.

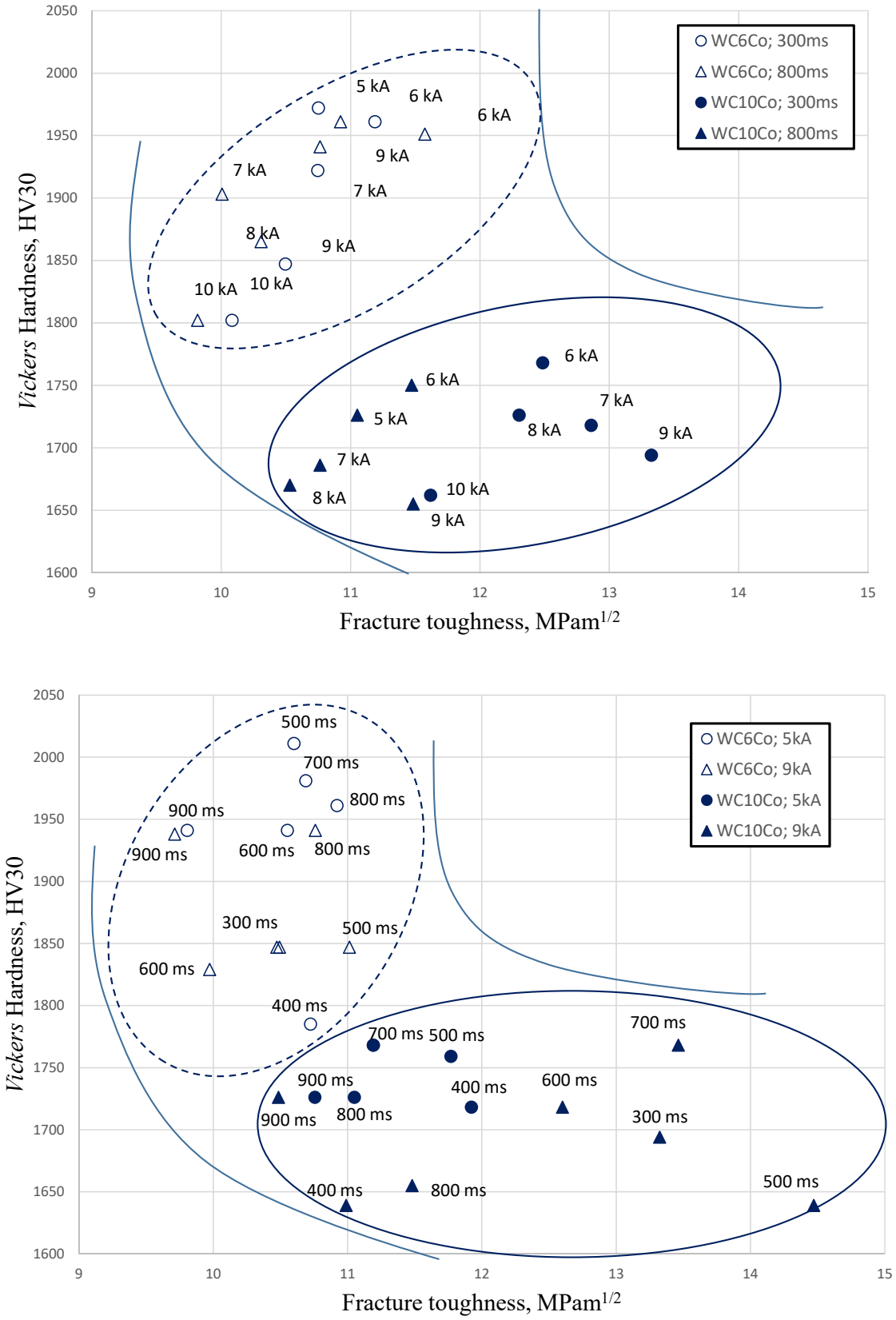

Fig. 4. Relationship between *Vickers* hardness and fracture toughness. Experiments carried out with a) 5-10 kA and b) 300-900 ms.

As previously shown, ERS may produce local sintering conditions (energy and temperature) that are not homogeneous through the whole sample. Density and mechanical properties of sintered compacts will consequently vary in different zones of the pellet (core and surfaces in contact with punches and with ceramic die). Fig. 5 shows optical images of the indentation cracks in three different zones of the compacts for WC-6Co (10 kA and 800 ms) and WC-10Co (8 kA and 800 ms). It can be seen that crack size depends not only on the region of the compact, but also on the growth direction. For instance, bigger cracks are found in the bases (radial cracks– point 2) of the sintered compact, and in the lateral surface (axial cracks – point 4). On other hand, in the core (point 5) the cracks have an intermediate behaviour, with a more homogenous size. From now on, the term radial toughness will be used related to toughness value computed from crack length growing in the radial direction, the other way around for axial toughness.

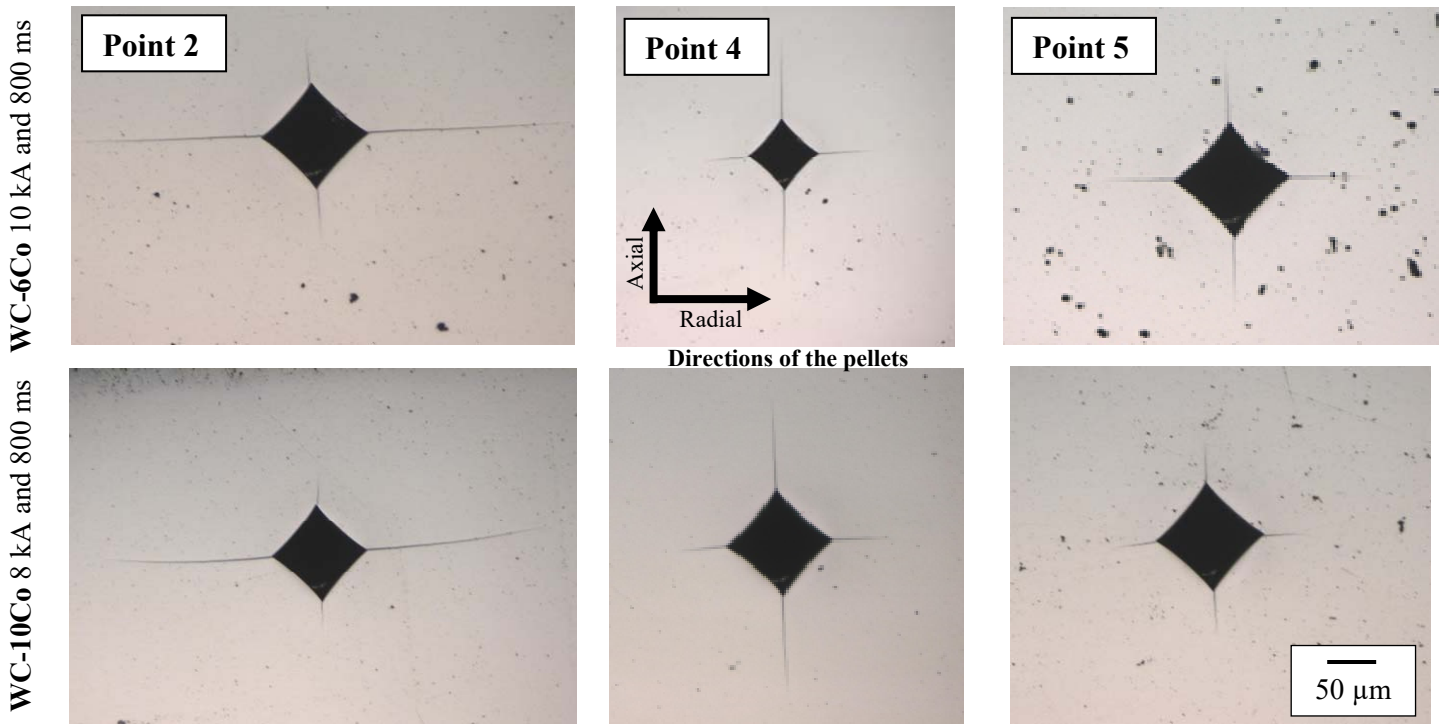

Fig. 5. Optical images of *Palmqvist* cracks induced from the corners of the *Vickers* indentations at different points (see scheme in Fig. 2) of an axial section of the WC-Co grades studied.

Fig. 6 shows fracture toughness values in radial and axial directions of the pellet (see details in figure 5), depending on the binder phase content, sintering conditions (current and time) and compact zones (points 2 and 4). In point 2 (closed symbols in the legend) all the K_{Ic} values in radial direction are lower than in axial direction (values appear bellow the dashed line), while a contrary trend is observed in point 4 (open symbols). The detailed analysis of these results allows us to suggest an anisotropic behaviour of the fracture toughness, whatever the material, sintering current or time.

This behaviour can be associated to the presence of residual stresses originating during the ERS process or to microstructural anisotropy. Residual stress value and sign (tensile or compression), as well as their distribution, depends on the energy supplied during the process (compaction pressure, sintering current and time), and the corresponding local temperature reached, the mechanism and the heat evacuation rate. According to the measured values, tensile residual stresses could have been generated during the sintering process in the axial direction, or compression in the radial direction, at the base of the pellets (point 2). The opposite would have occurred on the cylindrical surface of the compact (point 4). However, the presence of anisotropy in point 5 can be considered negligible. On the other hand, microstructural anisotropy (carbide size, embrittlement of the binder phase, mean free path of Co, etc.), could be related to phenomena (diffusion and dissolution/precipitation of ceramic phase) that depend on the value and distribution of the energy (temperature and pressure) in the compact during sintering.

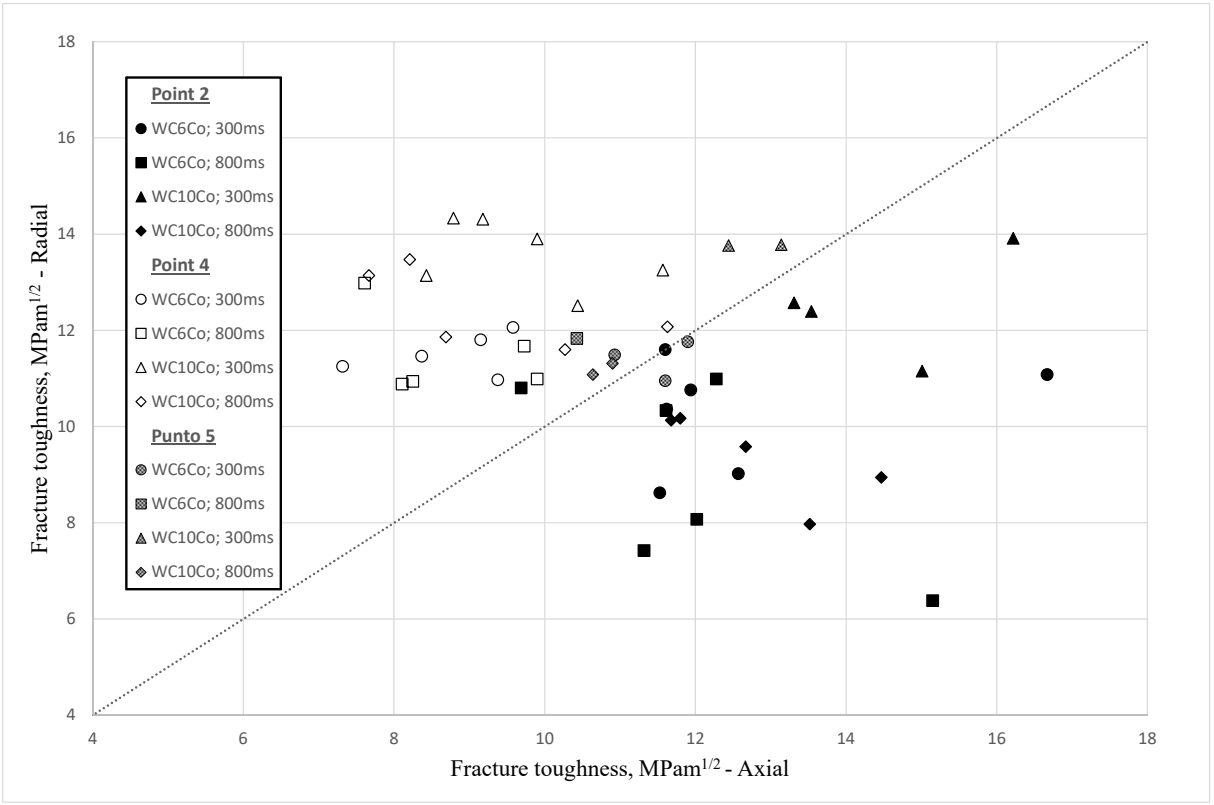

Fig. 6. Relationship between the fracture toughness measured in different zones and crack growth directions. The different values with the same symbol correspond to current intensities varying from 5 to 10 kA.

Within the framework of the results presented above, some of the possible causes of the mechanical anisotropy are studied next: 1) processing technique, 2) type of electrically insulating die, 3) microstructural anisotropy (d_{WC}, size and ductility of the binder phase), and 4) presence of residual stress (tensile and/or compression).

Influence of the processing technique

It is worth initially noting that this anisotropic behavior has not been reported in the literature for commercial cemented carbides manufactured by conventional powder metallurgy (PM) technology [23,34]. In order assess this behavior, the hardness and fracture toughness of samples obtained by ERS and by industrial PM practice of commercial powders (16F and 16M, supplied by Durit Ibérica S.L.) have been measured (see Table 4). ERS sintering conditions of 7 kA, 600 ms and 100 MPa, and study points 2, 4 and 5 were selected for these experiments. Results corroborate that in general the porosity and fracture toughness depend on the zone of the compact (core or surfaces), i.e., the anisotropic mechanical behavior is characteristic of the ERS technique, independently of the type of powder investigated (see Table 4 and Fig. 7). In general, toughness values in the sample core after ERS processing are similar to those obtained in compacts manufactured by conventional PM techniques. In addition, the density of Durit pellets is lower than for WC-10Co (ρ = 11.2 g/cm^3), for similar ERS condition. The above discrepancy may be associated with the higher carbide size and the content of carbon and oxygen of the commercial powder. Finally, the density reached for both techniques are coherent with the tendencies of the mechanical properties, being the hardness lower (K_{Ic} higher) for the electric sintering route.

Table 4. Density, *Vickers* hardness and fracture toughness in commercial grades obtained by ERS (7 kA, 600 ms and 100 MPa) and by conventional PM route [34]. **Notes:** 1) the average values of K_{Ic} are indicated in the table (*) and 2) including the outer porous layer (**)

			16F				**16M**			
			ERS		**PM**		**ERS**		**PM**	
Density (g/cm^3)			8.92**		14.6 ± 0.1		8.95**		14.5 ± 0.2	
HV30 (GPa)	**Point 2**		11.90		13.0 ± 1.1	15.4 ± 2.5	14.85		14.5 ± 1.2	14.0 ± 2.6
	Point 4		12.79				15.16			
	Point 5		14.21				13.45			
Fracture Toughness (MPa m$^{1/2}$)	**Point 2**	**Radial**	3.0	8.6*	11.1 ± 3.8	10.6 ± 0.9	3.8	10.6*	13.6 ± 4.5	15.3 ± 0.8
		Axial	14.3				17.5			
	Point 4	**Radial**	14.2	13.2*			14.8	15.1*		
		Axial	12.1				15.4			
	Point 5	**Radial**	11.1	11.4*			14.6	15.0*		
		Axial	11.8				15.5			

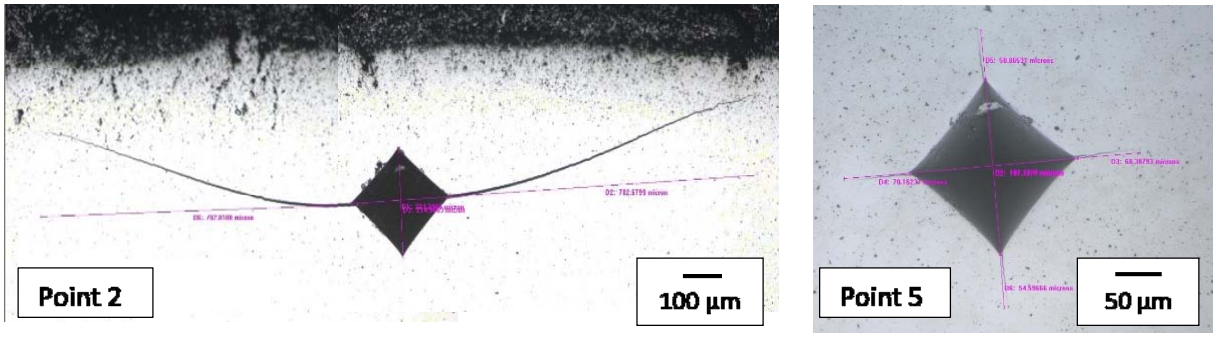

Fig. 7. Indentation cracks on a pellet obtained by ERS using commercial powder (16M grade).

Effect of the insulating die

The influence of the insulating die (alumina vs sialon) has also been evaluated. Results show anisotropy whatever the die type is. Nevertheless, the fracture toughness values at points 2 and 4 on both cemented carbide grades (at 9 kA and 600 ms) reveal an increase in anisotropy when using the sialon die, reaching increases in point 2 closed to 950% and 300% for WC-6Co and WC-10Co, respectively, while at point 4 are approximately 213% and 158%. This difference could be related to the thermal properties of the ceramic die, with a higher thermal conductivity in the sialon, which provokes a higher heat evacuation and lower temperatures as compared with the sample core.

Presence of microstructural anisotropy

Thirdly, the distribution of carbides size in the relevant zones and directions (radial and axial) of the compact were measured in detail (see Fig. 8). In addition, the characteristics of the path followed by the indentation cracks were studied (see Fig. 9). The influence of the microstructure on the fracture toughness may be accounted for by considering the effective bridging of the ductile ligament and the cracks deflection (intrinsic to big enough carbides) as prominent and operative toughening mechanisms. Bridging is dictated by the constraint generated by the WC and the ability of plastic stretching of the ligaments of Co. Furthermore, crack deflection is related to the presence of carbides (usually big carbides) [35,36]. Normally, in WC-Co the crack paths are transgranular through either the binder phase, although close to the carbide-binder interface, or the carbides [12,14,35]. The literature reports the estimation of the crack deflection effects on the nominal mode I stress intensity factor, using a simple micromechanical model proposed by Suresh [37]. There has been also reported the prominence of crack deflection as another operative toughening mechanism intrinsic to coarser carbides [30]. However, it is interesting to note that a crack-microstructure interaction is relatively uncommon in finer-grained hardmetals. i.e. crack deflection. As a result of the influence of metallic phase and crack deflection, hardmetals are expected to develop crack growth resistance (R-curve) behaviour. WC-Co cemented carbides exhibit a short in length but quite steep R-curve behaviour [35,38,39]. The toughening mechanisms depends on service conditions, for example the ductile ligaments are susceptible to be mechanically degraded under cyclic loading, while the presence and effectiveness of crack deflection as toughening mechanism is not affected by fatigue [19,40].

Fig. 8 allows to discern the presence of microstructural anisotropy, visualized as axial/radial curves separation, being slightly higher at points 2 and 4 than at point 5. Moreover, the differences in carbide grain size (different points and directions), as well as their potential influence on the crack deviation (toughening mechanisms) should be analysed in detail in probabilistic terms. The probability of finding carbides with an appropriate size to generate the crack deviation phenomenon is different and depends on the zone and the direction evaluated. In the context of the above discussion, we can observe that it is very different the probability (frequency) that has a fissure to find on its way WC with an average size of 290-300 nm, depending on the direction of propagation (radial or axial), as well as the pellet zone (core or surfaces). A similar analysis can be made for a constant probability (for example, 50%); in this case it can be observed that there is a greater range of carbides sizes (greater influence of the mechanism of deviation of the crack) in points 2 and 4, zones of the pellets with significant differences in mechanical behaviour.

For instance, the number of carbides larger than 290-300 nm that will preferentially produce a crack path diversion depends on the pellet zone and direction of propagation, as follows: point 2 (33% - axial vs 51%-radial), point 4 (29% - axial vs 43%-radial) and point 5 (42% - axial vs 54%-radial). So, concerning the toughening mechanism of crack deflexion, radial toughness would be always greater than axial value; point 4 should show bigger toughness values, and anisotropy would be higher at points 2 and 4 than at point 5. These considerations are only partially supported by measured toughness values (see Fig. 6). Mean toughness value at point 4 is not the highest, but at points 2 and 4. Radial toughness is greater than axial value at point 4 and possibly 5, but not at point 2. It is true that anisotropy is lower at point 5. As a consequence, these results point out that other mechanisms, like those suggested in the next paragraph, should be active in determining mechanical behaviour.

On the other hand, the study of deformation phenomena (slip and twinning traces, as well as induced phase transformation of the binder from the metastable fcc structure to the stable hcp one) and the residual stress profile within the binder phase, required for supporting such a hypothesis, warrants an additional detailed study of transmission electron microscopy, electron back scattered diffraction (EBSD) and neutron diffraction, which is however out of the scope of this work.

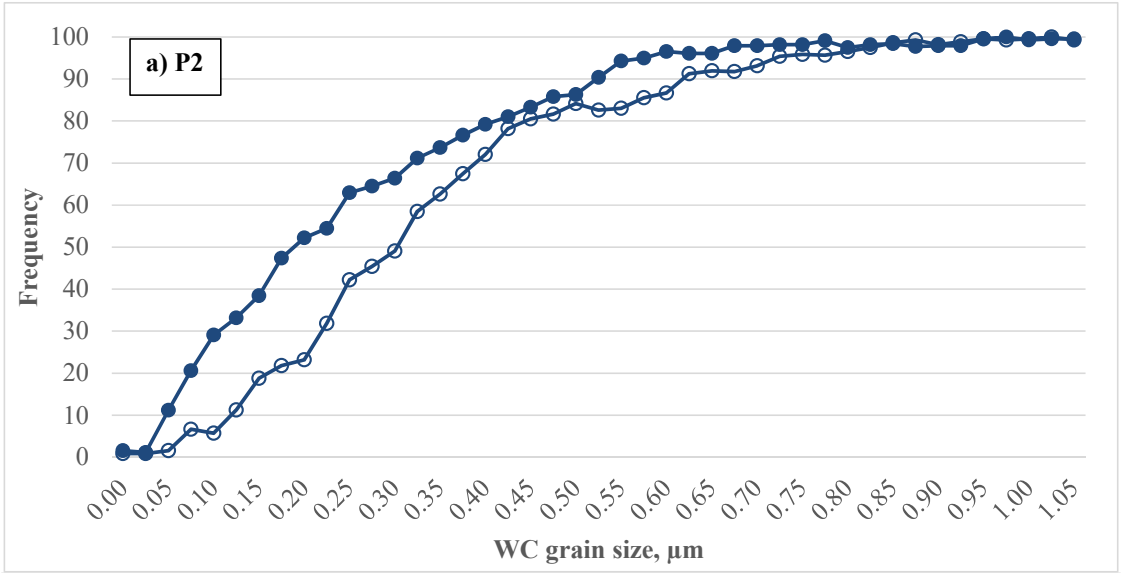
a) P2
Frequency
WC grain size, µm

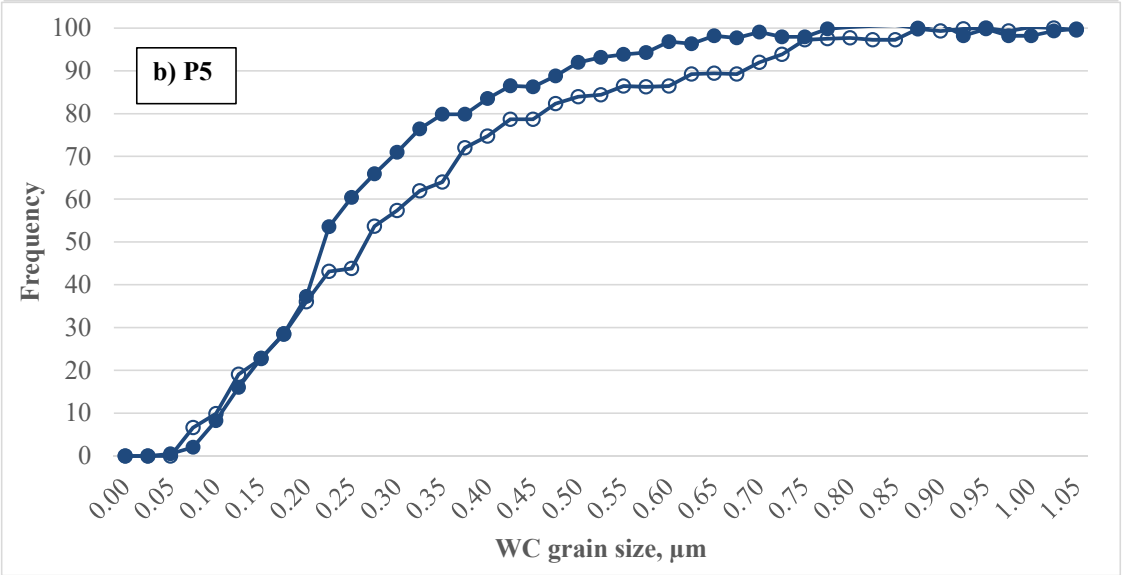
b) P5
Frequency
WC grain size, µm

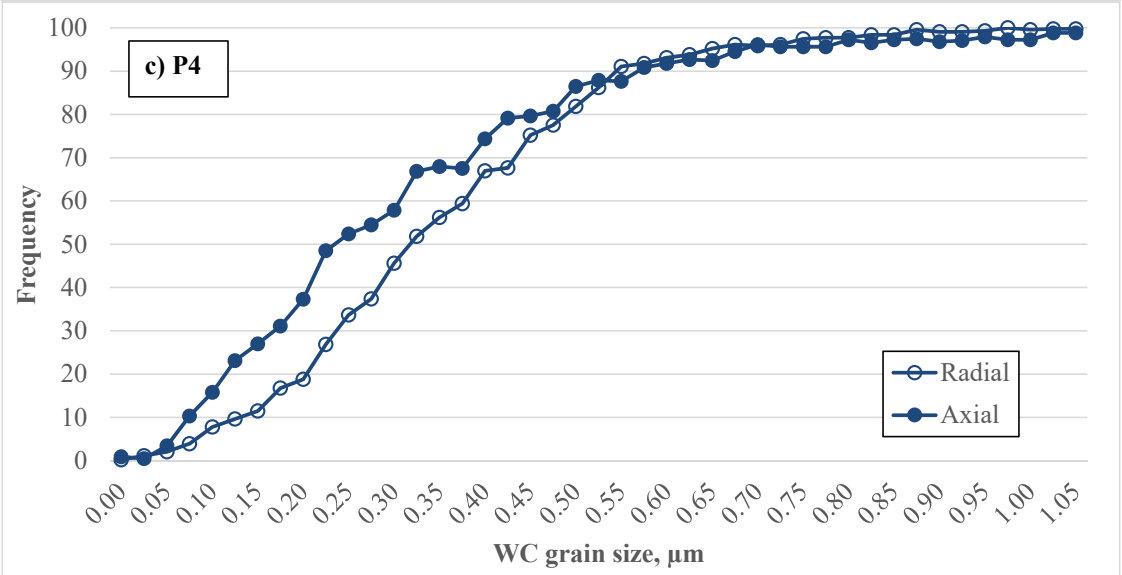
c) P4
Frequency
WC grain size, µm
Radial
Axial

Fig. 8. WC grain size distribution. Comparison between the radial and axial directions of a WC10Co sample sintered at 9 kA for 600 ms at: a) point 2 (sample base), b) point 5 (sample core), and c) point 4 (sample lateral surface).

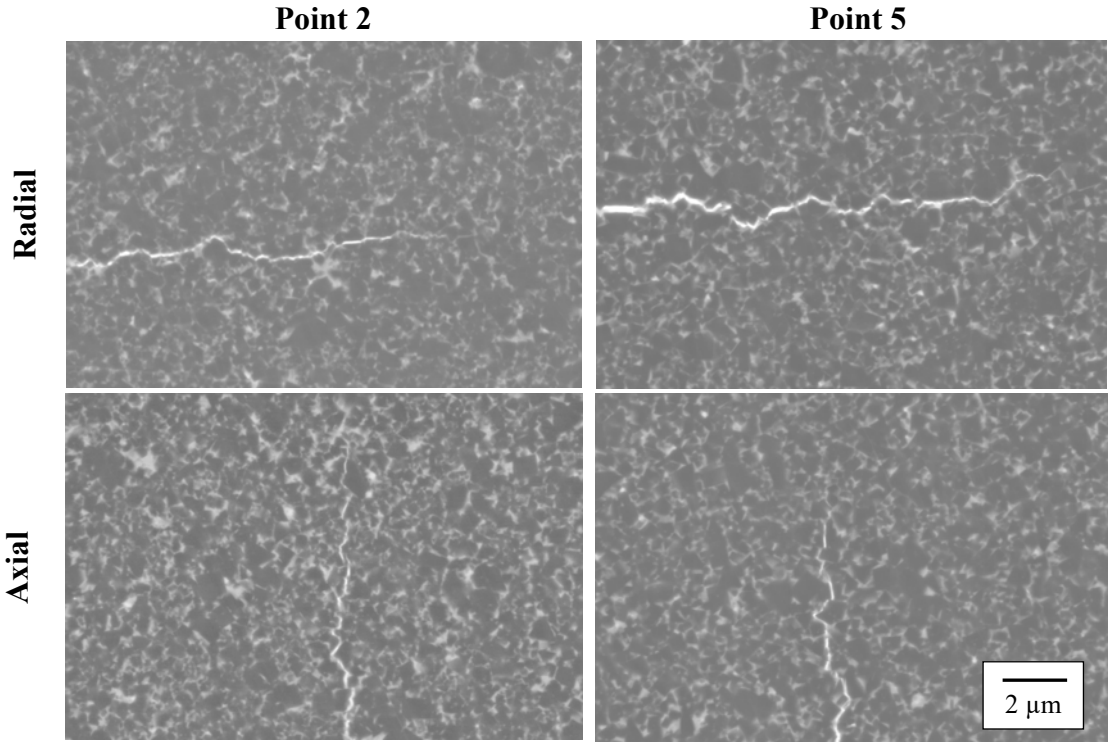

Fig. 9. Features of the path of indentation cracks in the area near their tip. Study for the radial and axial direction, in points 2 and 5 of WC-10Co grade sintered at 7 kA during 800 ms.

In general, the SEM images shown in Fig. 9 indicate that the indentation cracks are fine, sharp and with periodic tilts. It is therefore suggested that the crack growth proceeds through a compromising scenario: crack deflection through metallic binder paths and transgranular carbides cracking (particularly for some large carbides). As a result, crack paths are rather tortuous (non planar), mainly following the metallic binder, but exhibiting pronounced and frequent deflections. In this scenario, straighter paths could be expected in the zones and directions with tensile, crack-opening residual stresses, while tortuous paths will occur in the absence of these stresses (or the presence of compressive stresses).

Study of the presence of residual stresses

Table 5 and Fig. 10 show the fracture toughness values obtained after carrying out residual stress relief (RSR) and/or additional ERS pulse (AP) treatments. The RSR treatment has been made in a Carbolite® STF 15/75/450 ceramic furnace with a horizontal tube, at 800ºC for 2 h using high vacuum (~5 × 10-5 mbar), while the AP consisted in a second train of sintering after the main sintering pulse, in this case at low intensity (1 kA) during 300 ms. These results allow to evaluate the presence of residual stresses and their influence on the mechanical behaviour. In this context, some conclusions can be withdrawn: 1) as shown in Figure 10a by the values after the RSR treatment being nearer the divisor line, the mechanical anisotropy decreases after the RSR, whatever the WC-Co grade or the pellet zone, 2) the fracture toughness decreases slightly after heat treatment, 3) as shown in Fig. 10b, applying an AP is not recommended (the residual stresses increase), 4) neither the use of AP and RSR significantly improve the final results, and 5) the magnitude and type (tensile or compression) of the residual stresses accumulated during the manufacture of the pellets depend on the sintering conditions, the area of the sample (bases and the lateral surface) and the binder content of the cemented carbide. Note that the residual stresses (associated with ERS) are generally greater in the surface of the pellets. However, in this work it is recommended to

carry out in the future a more detailed analysis (statistically representative) that allows establishing and studying these trends, as well as the type of residual stress [41-44].

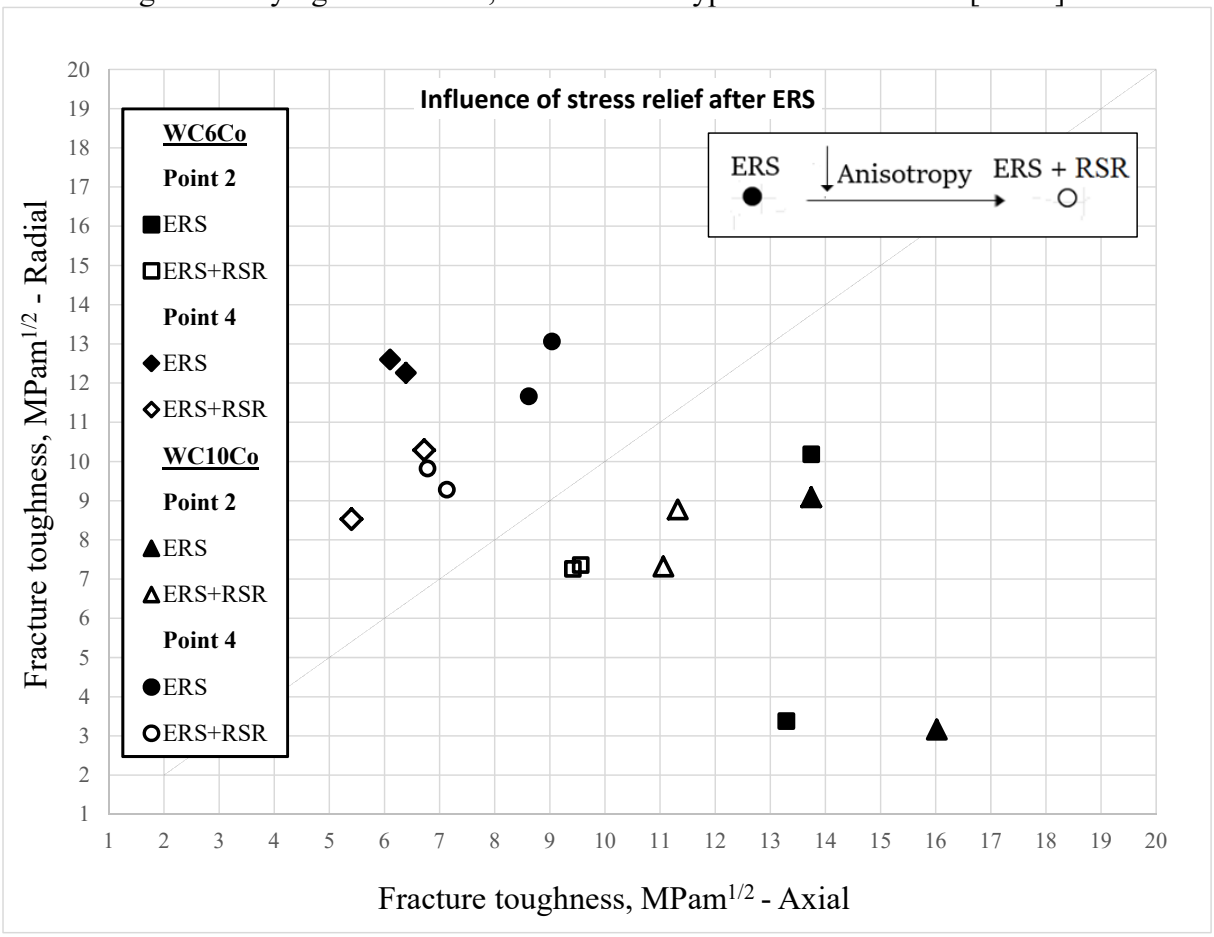

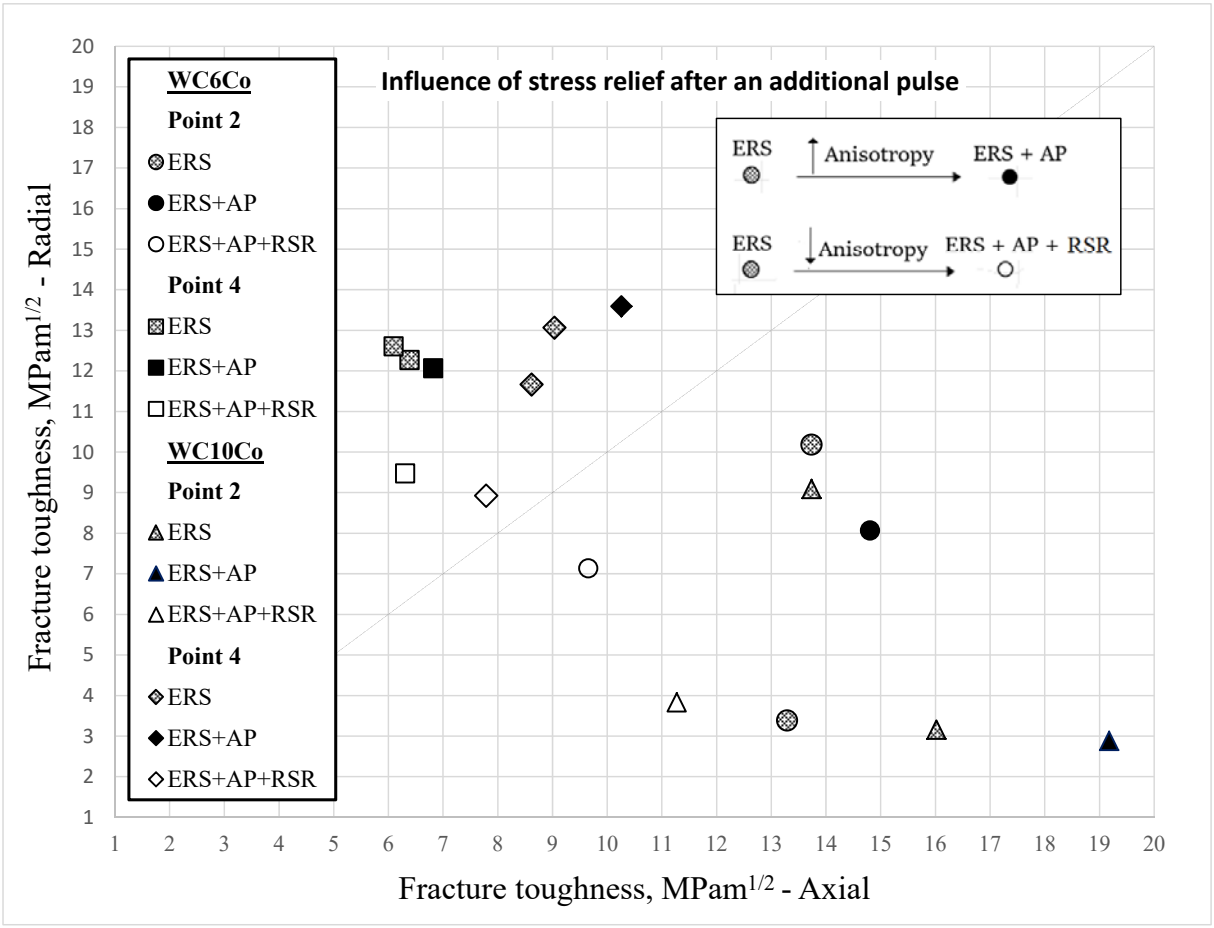

Fig. 10. Influence of AP and RSR treatments in the anisotropic mechanical behavior.

Table 5. Influence of residual stress relief treatments on *Vickers* hardness and fracture toughness.

			WC-6Co						**WC-10Co**					
			7 kA-700 ms		7 kA-600 ms				7 kA-700 ms		7 kA-800 ms			
			ERS	ERS + RSR	ERS	ERS + RSR	ERS + AP	ERS + AP + RSR	ERS	ERS + RSR	ERS	ERS + RSR	ERS + AP	ERS + AP + RSR
Density (g/cm^3)			10.8	10.8	11.1	11.1	10.9	10.9	10.9	10.9	10.8	10.8	10.8	10.8
Hardness HV30 (GPa)	Point 2		15.4	20.3	19.8	20.0	20.9	20.1	14.0	18.3	18.6	18.6	13.0	16.6
	Point 4		17.1	20.5	20.1	20.1	20.6	20.2	18.6	18.4	18.5	18.3	18.6	18.2
Fracture Toughness (MPam$^{1/2}$)	Point 2	Radial	3.4	7.4	10.2	7.3	8.1	7.1	3.2	8.8	9.1	7.3	2.9	3.8
		Axial	13.3	9.6	13.7	9.4	14.8	9.7	16.0	11.3	13.7	11.1	19.2	11.3
	Point 4	Radial	12.6	10.3	12.3	8.5	12.1	9.5	13.1	9.3	11.7	9.8	13.6	8.9
		Axial	6.1	6.7	6.4	5.4	6.8	6.3	9.0	7.1	8.6	6.8	10.3	7.8

CONCLUSIONS

In this work two WC-Co grades obtained using the ERS technique were investigated. Based on the main findings of the study, the following conclusions may be drawn:

1) The ERS is a fast processing route. This technique is currently effective to obtain simple pieces or preforms of cemented carbides (WC-Co). The physical (density) and mechanical properties (hardness and fracture toughness) of the manufactured materials depend on the energy supplied during the electric sintering. This energy depends on the process parameters (sintering current and time, die materials, applied pressure, etc.).

2) The fracture toughness of these WC-Co depends on the role played by the cobalt ligaments and the deviation of the crack associated to the presence of the WC carbides (toughening mechanisms / R-curve behavior).

3) Electrically sintered WC-Co pellets present residual stresses, porosity and small microstructural changes (carbide grain size and cobalt binder thickness). These differences depend on the zone (bases and the lateral surface) and the direction (radial or axial), being the responsible of the anisotropy of the fracture toughness of the WC-Co pellets obtained by ERS.

4) The anisotropy of the mechanical behaviour is greater if additional electrical pulses are applied, while this heterogeneity is negligible if an adequate heat treatment of the WC-Co pellets is carried out following the ERS.

5) Whatever the WC-Co grade studied, in this work the following manufacturing process of the pellets is recommended: electric sintering (7 kA, 600 ms and 100 MPa, in an cylindrical alumina die), and then a relief treatment of residual stresses (800 ºC, 2 h and high vacuum). This recommendation is made in terms of the best balance of structural integrity, density, homogeneity and mechanical behaviour (*Vickers* hardness and K_{Ic}) of the pellets.

ACKNOWLEDGEMENTS

The authors are grateful to EU for funding this research within the framework of the EU 7th Framework FoF.NMP.2013-10 608729 EFFIPRO Project. We also thank the Microscopy Central Service (CITIUS, University of Seville). Finally, the authors would like to thank technicians J. Pinto, M. Sánchez and M. Madrid for assistance in microstructural and micro-mechanical testing.

REFERENCES

[1] G.S. Upadhyaya, Cemented tungsten carbides: Production, Properties and Testing, Noyes Publications, New Jersey, USA, 1998.

[2] L.J. Prakash, Fundamentals and general applications of hardmetals, in: V. K. Sarin, D. Mari, L. Llanes (Eds.), Comprehensive Hard Materials, Elsevier, UK, 2014, pp.29–90.

[3] J. García, V. Collado, A. Blomqvist, B. Kaplan, Cemented carbide microstructures: a review, Int. J. Refract. Met. Hard Mater. 80 (2019) 40–68

[4] R. Orrù, R. Licheri, A.M. Locci, A. Cincotti, G. Cao, Consolidation/synthesis of materials by electric current activated/assisted sintering, Mater Sci Eng, R: Reports. 63 (2009) 127–287.

[5] S. Grasso, Y. Sakka, G. Maizza, Electric current activated/assisted sintering (ECAS): a review of patents 1906–2008, Sci. Technol. Adv. Mater. 10 (2009) 1–24, doi:10.1088/1468-6996/10/5/053001.

[6] K. Okazaki, Electro-discharge consolidation of particulate materials, Rev. Part. Mater. 2 (1994) 215–269.

[7] G. L. Burenkov, A. I. Raichenko, A. M. Suraeva, Macroscopic mechanism of formation of interparticle contact in electric current sintering of powders, Sov. Powder Metall. Met. Ceram. 28 (1989) 186–191, doi:10.1007/BF00794794.

[8] J. R. Groza, A. Zavaliangos, Sintering activation by external electrical field, Mater. Sci. Eng. A 287 (2000) 171–177.

[9] J. M. Montes, J. A. Rodríguez, F. G. Cuevas, J. Cintas, Consolidation by electrical resistance sintering of Ti powder, J. Mater. Sci. 46 (2011) 5197–5207.

[10] H.E. Exner, Physical and chemical nature of cemented carbides, Int. Met. Rev. 24 (1979) 149–173.

[11] S. Lay, J.-M. Missiaen, Microstructure and morphology of hardmetals, Comprehensive Hard Materials, Elsevier, UK 2014, pp. 91–120.

[12] R.K. Viswanadham, T.S. Sun, E.F. Drake, J.A. Peck, Quantitative fractography of WC–Co cermets by Auger spectroscopy, J. Mater. Sci 16 (1981) 1029–1038.

[13] V.D. Krstic, On the fracture of brittle-matrix/ductile-particle composites, Philos Mag 48 (1983) 695–708.

[14] L.S. Sigl, H.E. Exner, Experimental study of the mechanics of fracture in WC–Co alloys, Metall. Trans. A. 18A (1987) 1299–308.

[15] L.S. Sigl, H.F. Fischmeister, On the fracture toughness of cemented carbides, Acta Metall. 36 (1988) 887–97.

[16] L.S. Sigl, P.A. Mataga, B.J. Dalgleish, R.M. McMeeking, A.G. Evans, On the toughening of brittle materials reinforced with a ductile phase, Acta Metall. 36 (1988) 945–53.

[17] B. Roebuck, E.A. Almond, Deformation and fracture processes and the physical metallurgy of WC–Co hardmetals, Int. Mater. Rev. 33 (1988) 90-112.

[18] L.L. Shawa, H. Luob, Y. Zhonga, WC-18 wt.% Co with simultaneous improvements in hardness and toughness derived from nanocrystalline powder, Mater. Sci. Eng. A 537 (2012) 39–48.

[19] L. Llanes, Y. Torres, M. Anglada, On the fatigue crack growth behavior of WC–Co cemented carbides: kinetics description, microstructural effects and fatigue sensitivity, Acta Mater, 50 (2002) 2381–93.

[20] A.J. Ganta, R. Morrell, A.S. Wronski, H.G. Jones, Edge toughness of tungsten carbide based hardmetals, Int. J. Refract. Met. Hard Mater. 75 (2018) 262–278.

[21] B. Roebuck, M. G. Gee, R. Morrell, Developments in testing and mechanical properties of hard materials, Powder Metall. 39 (1996) 213-218.

[22] M. N. James, A. M. Human, S. Luyckx, Fracture toughness testing of hardmetals using compression-compression precracking, J. Mater. Sci. 25 (1990) 4810-14.

[23] Y. Torres, D. Casellas, M. Anglada, L. Llanes, Fracture toughness evaluation of hardmetals: influence of testing procedure, Int. J. Refract. Met. Hard Mater. 19 (2001) 27–34.

[24] ISO 28079:2009 Hardmetals-Palmqvist toughness test. STANDARD by British Standard/International Organization for Standardization (2009).

[25] S. Sheikh, R. M'Saoubi, P. Flasar, M. Schwind, T. Persson, J. Yang, L. Llanes, Fracture toughness of cemented carbides: Testing method and microstructural effects, Int. J. Refract. Met. Hard Mater. 49 (2015) 153–160.

[26] C. B. Ponton, R. D. Rawlings, Vickers indentation fracture toughness test, part 1: review of literature and formulation of standardised indentation toughness equations, Mater. Sci. Technol. 5 (1989) 865-872.

[27] H.E. Exner, The influence of sample preparation on Palmqvist's method for toughness testing of cemented carbides, Trans Met Soc AIME, 245 (1969), 677-683.

[28] J. M. Montes, J. Cintas, F. G. Cuevas, J. A. Rodriguez, Electrical resistance sintering of M.A. Al-5AlN powders, Mater. Sci. Forum (2006) 514–516.

[29] ISO 3369:2006 Impermeable sintered metal materials and hardmetals – Determination of density. STANDARD by International Organization for Standardization (2006).

[30] ISO 3878:1983 Hardmetals – Vickers hardness test. STANDARD by International Organization for Standardization (1983).

[31] B. Roebuck, E.G. Bennett, Phase size distribution in WC–Co hardmetal, Metallography 19 (1986) 27–47.

[32] S. Luyckx, A. Love, The dependence of the contiguity of WC on Co content and its independence from WC grain size in WC–Co alloys, Int. J. Refract. Met. Hard Mater. 24 (2006) 75–79.

[33] J.M. Tarragó, D. Coureaux, Y. Torres, F.Wu, I. Al-Dawery, L. Llanes, Implementation of an effective time-saving two-stage methodology for microstructural characterization of cemented carbides, Int. J. Refract. Met. Hard Mater. 55 (2016) 80–86.

[34] Y. Torres, Comportamiento a fractura y fatiga de carburos cementados WC-Co. (PhD Thesis) Universitat Politècnica de Catalunya, Barcelona (2002).

[35] J.M. Tarragó, E. Jiménez-Piqué, L. Schneider, D. Casellas, Y.Torres, L. Llanes, FIB/FESEM experimental and analytical assessment of R-curve behavior of WC–Co cemented carbides, Mater. Sci. Eng. A 645 (2015) 142–149.

[36] Y. Torres, J.M. Tarragó, D. Coureaux, E. Tarrés, B. Roebuck, P. Chan, M. James, B. Liang, M.Tillman, R.K.Viswanadham, K.P. Mingard, A. Mestra, L. Llanes, Fracture and fatigue of rock bit cemented carbides: Mechanics and mechanisms of crack growth resistance under monotonic and cyclic loading, Int. J. Refract. Met. Hard Mater, 45 (2014) 179-188.

[37] S. Suresh, Fatigue crack deflection and fracture surface contact: micromechanical models, Metall. Trans., 16A (1985) 249–260.

[38] J.M. Tarragó, D. Coureaux, Y. Torres, D. Casellas, I. Al-Dawery, L. Schneider, L. Llanes, Microstructural effects on the R-curve behavior of WC-Co cemented carbides, Mater. Des. 97 (2016) 492–501.

[39] J.M. Tarragó, D. Coureaux, Y. Torres, E. Jiménez-Piqué, L. Schneider, J. Fair, L. Llanes, Strength and reliability of WC-Co cemented carbides: Understanding microstructural effects on the basis of R-curve behavior and fractography, Int. J. Refract. Met. Hard Mater, 71 (2018) 221–226.

[40] Th. Sailer, M. Herr, H.G. Sockel, R. Schulte, H. Feld and L.J. Prakash, Microstructure and mechanical properties of ultrafine-grained hardmetals, Int. J. Refract. Met. Hard Mater. 19 (2001) 553-559.

[41] A. Krawitz, E. Drake, Residual stresses in cemented carbides - An overview, Int. J. Refract. Met. Hard Mater. 49 (2015) 27-35.

[42] B. Casas, A. Lousa, J. Calderón, M. Anglada, J. Esteve, L. Llanes, Mechanical strength improvement of electrical discharge machined cemented carbides through PVD (TiN, TiAlN) coatings, Thin Solid Films, 447-448 (2004) 258-63.

[43] S. Farag, I. Konyashin, B. Ries, The influence of grain growth inhibitors on the microstructure and properties of submicron, ultrafine and nano-structured hardmetals – A review, Int. J. Refract. Met. Hard Mater. 77 (2018) 12-30.

[44] J. Yang, J.J Roa, M. Schwind, M. Odén, M.P. Johansson-Jõesaar, J. Esteve and L. Llanes, Thermally induced surface integrity changes of ground WC-Co hardmetals, Procedia CIRP 45 (2016) 91-94.

Figure Captions

Fig. 1. SEM images of the powders used for the sintering of hardmetals.

Fig. 2. Structural integrity (photographs) and porosity distribution (optical images – axial surfaces) of the pellets obtained in well apart sintering conditions with the alumina die.

Fig. 3. SEM images of the microstructure of the WC-Co blank core studied (point 3 in the scheme in Figure 2). Influence of sintering time in WC-6Co and 5 kA [a) and b)] and sintering current for WC-10Co and 400 ms [c) and d)].

Fig. 4. Relationship between Vickers hardness and fracture toughness. Experiments carried out with a) 5-10 kA and b) 300-900 ms.

Fig. 5. Optical images of Palmqvist cracks induced from the corners of the Vickers indentations at different points (see scheme in Fig. 2) of an axial section of the WC-Co grades studied.

Fig. 6. Relationship between the fracture toughness measured in different zones and crack growth directions. The different values with the same symbol correspond to current intensities varying from 5 to 10 kA.

Fig. 7. Indentation cracks on a pellet obtained by ERS using commercial powder (16M grade).

Fig. 8. WC grain size distribution. Comparison between the radial and axial directions of a WC10Co sample sintered at 9 kA for 600 ms at: a) point 2 (sample base), b) point 5 (sample core), and c) point 4 (sample lateral surface).

Fig. 9. Features of the path of indentation cracks in the area near their tip. Study for the radial and axial direction, in points 2 and 5 of WC-10Co grade sintered at 7 kA during 800 ms.

Fig. 10. Influence of AP and RSR treatments in the anisotropic mechanical behavior.

Table Captions

Table 1. Chemical composition and properties of the starting powders supplied by Kyocera Unimerco (Denmark).

Table 2. Experimental parameters associated to the electrical resistance sintering of the studied WC-Co.

Table 3. Experimental parameters of the microstructure of WC-Co studied.

Table 4. Density, Vickers hardness and fracture toughness in commercial grades obtained by ERS (7 kA, 600 ms and 100 MPa) and by conventional PM route [26]. Notes: 1) the average values of KIc are indicated in the table (*) and 2) including the outer porous layer (**).

Table 5. Influence of residual stress relief treatments on Vickers hardness and fracture toughness.